

Design, fabrication, and verification of a three-dimensional autocollimator

YANHE YIN,^{1,2} SHENG CAI,^{1,*} AND YANFENG QIAO¹

¹Changchun Institute of Optics, Fine Mechanics and Physics, Chinese Academy of Sciences, Changchun 130033, China

²University of Chinese Academy of Sciences, Beijing 100049, China

*Corresponding author: cais_ciomp@hotmail.com

Received 9 August 2016; revised 17 October 2016; accepted 1 November 2016; posted 2 November 2016 (Doc. ID 270609); published 5 December 2016

The autocollimator is an optical instrument for noncontact angle measurement with high resolution and a long detection range. It measures two-dimensional angles, i.e., pitch and yaw, but not roll. In this paper, we present a novelly structured autocollimator capable of measuring three-dimensional (3D) angles simultaneously. In this setup, two collimated beams of different wavelengths are projected onto a right-angle prism. One beam is reflected by the hypotenuse of the prism and received by an autocollimation unit for detecting pitch and yaw. The other is reflected by the two legs of the right-angle prism and received by a moiré fringe imaging unit for detecting roll. Furthermore, a prototype is designed and fabricated. Experiments are carried out to evaluate its basic performance. Calibration results show that this prototype has angular RMS errors of less than 5 arcsec in all 3Ds over a range of 1000 arcsec at a working distance of 2 m. © 2016 Optical Society of America

OCIS codes: (120.3940) Metrology; (120.0120) Instrumentation, measurement, and metrology; (120.4120) Moiré techniques; (120.0280) Remote sensing and sensors.

<https://doi.org/10.1364/AO.55.009986>

1. INTRODUCTION

Since its appearance nearly a century ago [1], the autocollimator has been widely used in metrology and precise engineering for its simple structure and high accuracy [2–4]. For years, this instrument has been modernized with technique innovations. Recent improvements include using charge coupled devices (CCDs) as detectors, light-emitting diodes (LEDs) as light sources, and digital processing units to provide high-speed real-time angular monitoring [5–7]. Yet the basic structure of the autocollimator has barely changed.

Conventionally, when measuring the angular position of an object, an autocollimator has to work in conjunction with a reflector, for instance, a plane mirror attached to target. When the object's attitude changes, the mirror deflects with it and reflects the light beam in a different direction, and the autocollimator obtains the reflected beam and retrieves the angular information. This works for measuring pitch and yaw, but fails to acquire the roll angle around the visual axis (as shown in Fig. 1), which is also an important parameter in many applications. Facing this problem, one would naturally think of using a second autocollimator in a direction perpendicular to the first one, in which the original roll angle becomes a new pitch. However, this approach is not applicable under certain circumstances. For example, when measuring the three-dimensional (3D) angular deformation of a bridge-like structure, placing a

second autocollimator in the perpendicular direction seems impossible. Sometimes even if a second autocollimator can be placed, such as when measuring the body deformation of a ship under harsh conditions on the sea, the pitch from the second autocollimator differs from the original roll because of the rotation. In these cases, an autocollimator that simultaneously measures 3D angles is in crucial need.

Konyakhin and Turgalieva [8] try to solve this problem by using a tetrahedral prism instead of the plane mirror as the reflector and revising the algorithm without changing the structure of autocollimator. The method is simple and effective, though it is shy in accuracy. The RMS error of rotation measurement is 20 arcsec. Similarly, TRIOPTICS launched a new type of autocollimator named TriAngle 3D, which uses a right-angle prism instead of the plane mirror. It has a resolution of 1 arcsec and an accuracy of 5 arcsec for roll measurement. Recently, Yang Gao and colleagues [9] put forward an approach using a point array reticle and two identical collimators in contraposition, one as projector and the other as receiver. Simulations and experiments show satisfactory results; the RMS error of roll measurement is 0.39 arcsec. However, as no reflector is applied in this setup, half the device—that is, one collimation unit—has to be mounted onto the object, which seems difficult to realize when the target is small, for instance, a component in an optical setup. In another solution

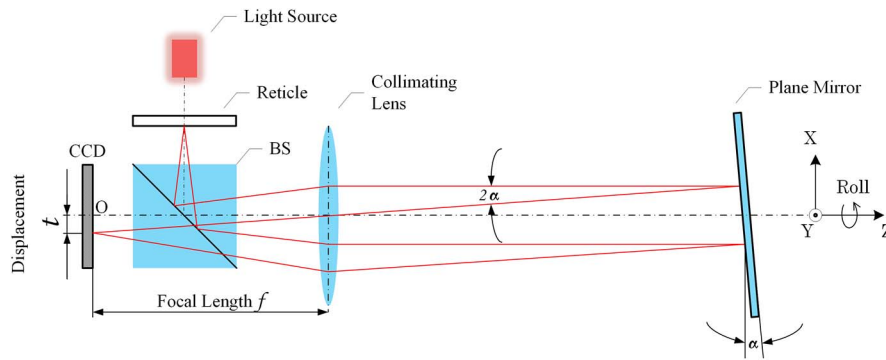


Fig. 1. Schematic of a standard autocollimator.

given by Wei Gao *et al.* [10], a grating is employed as the reflector. The reflected zeroth-order diffracted beam is received by an autocollimation unit for detecting the pitch and yaw, while the reflected first-order diffracted beam is received by another autocollimation unit for detecting the roll. A prototype has been made, and nonlinear error of the sensor is about 2.5 arcsec over a range of 40 arcsec.

In this paper we investigate the question of whether the principle of autocollimation and another well-developed solution for high-precision angle measurement—moiré technique—can be combined. We will show that these two methods can be perfectly integrated to measure 3D angles by sharing the same light path and collimating lens set when cooperating with a right-angle prism. In this setup, two collimated beams are projected to the right-angle prism; one is reflected by the hypotenuse and detected by an autocollimation unit. Based on the principle of autocollimation, the pitch and yaw angles will be converted into *y*- and *x*-directional linear displacements of the light spot on the detector, respectively, from which the pitch and yaw angles can be simultaneously detected. On the other hand, the other beam is reflected by the two legs of the right-angle prism and detected by a moiré imaging unit, by which the roll angle can be measured.

While our previous work [11] mainly focused on the principles and error analysis, this paper will concentrate on the system design, implementation, and experimental verification of the device. The remainder of the paper is organized as follows. In Section 2, the principles of autocollimation and moiré fringe are reviewed. Then, we describe the structure and how it works in Section 3. The experimental setup and results are given in Section 4. In the end, the conclusion and a brief mention of further development follow in Section 5.

2. PRINCIPLE

A. Standard Autocollimator

We first briefly sketch the basic schematic of a standard autocollimator. As shown in Fig. 1, a light source illuminates the reticle and produces an optical image, i.e., a crosshair. After passing through a beam splitter (BS), the light beam is collimated by the objective lens with a focal length *f*. Then the beam is projected onto a target mirror. The reflected light beam is collected by the same lens and refocused on the image plane, where the CCD camera is placed.

Assuming that the light beam travels along the *z* axis, the pitch, yaw, and roll are the angles about the *x*, *y*, and *z* axes, respectively. If the collimated beam falls onto the mirror perpendicularly, the beam is reflected back along its original path and is focused on the origin point *O*. If the target mirror is tilted with a pitch angle α around the *y* axis, the reflected beam is deflected through an angle 2α , and the image is displaced laterally from *O*. The amount of displacement is given by

$$t = f \tan 2\alpha. \tag{1}$$

Thus, the pitch angle can be obtained:

$$\alpha = \frac{1}{2} \arctan \frac{t}{f}. \tag{2}$$

Generally, the angle is small enough that Eq. (2) can be approximately written as

$$\alpha = \frac{t}{2f}. \tag{3}$$

Similarly, we have yaw angle β around the *x* axis:

$$\beta = \frac{t'}{2f}, \tag{4}$$

where *t'* is the displacement in the *y* direction. As the CCD camera detects the position of the crosshair on the two-dimensional image plane, the pitch and yaw angles can be simultaneously retrieved.

B. Moiré Fringe

Another wildly popular technique for small angle measurement is moiré technique. The word *moiré* stems from the description in French for watered silk forming an interfering pattern. Nowadays, a moiré fringe refers to any pattern that appears when two or more periodic patterns are superimposed with a small rotation angle. For example, as illustrated in Fig. 2, when two transparent gratings are laid one on the top of another in optical contact, a pattern of bright and dark stripes appears—that is, a moiré fringe. If the gratings are of a regular type, the moiré fringe is also regular.

The distance *w* depends on the grating constants *d*₁ and *d*₂ and deviation angle ϕ between the elements of two gratings as follows [12]:

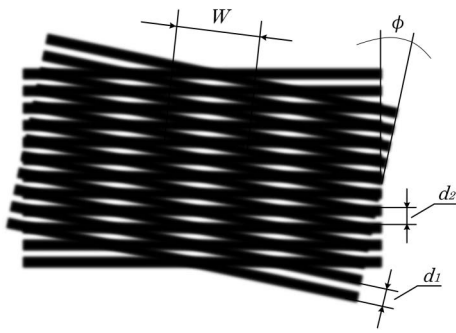


Fig. 2. Moiré fringes formed by two gratings. d_1 , d_2 , pitch of gratings; ϕ , angle of deviation; w , distance between fringes.

$$w = \frac{d_1 d_2}{\sqrt{d_1^2 + d_2^2 - 2d_1 d_2 \cos \phi}} \tag{5}$$

If the two gratings are equal to each other, the deviation angle ϕ will be

$$\phi = 2 \arcsin \frac{d}{2w}, \tag{6}$$

where $d = d_1 = d_2$ is the constant of the two gratings. As the small angle is amplified and transformed into a considerable stripe width, moiré technique provides high resolution and accuracy in the measurement. Now that we have an autocollimator to measure pitch and yaw, and moiré technique for the roll angle, the question is how to integrate them into a single device.

3. DESIGN AND FABRICATION

To incorporate autocollimation and moiré technique in the same light path while keeping them from interfering with each other, two light sources of different wavelengths, two band-pass (BP) filters and a specially coated right-angle prism are employed.

As shown in Fig. 3, when the light emitted from red LED passes through a reticle, a BS, and an objective lens in sequence, a collimated light beam with a crosshair image is formed. The beam is projected onto the hypotenuse surface of the right-angle prism and reflected back to a camera (CCD1). The

hypotenuse surface is coated to be reflective with red light and transmissive with green light. In this way, the right-angle prism works as a plane mirror for autocollimation. Obviously, this is exactly the same principle as described in Section 2.A, by which the pitch and yaw angles can be measured.

At the same time, the roll angle is indicated by the rib, which is the intersection of two legs of the right-angle prism. The green LED illuminates a sinusoidal amplitude grating and forms a light beam carrying the information of the grating. After passing through three BSs, an objective lens, and the hypotenuse surface of the right-angle prism, the beam is reflected by the two legs of the prism (as the hypotenuse is transmissive to green light). The reflected beam interferes with a second grating to form a moiré fringe to be detected by another camera (CCD2). Two filters are placed in front of the CCD cameras to ensure the red light and green light are separate.

Using the matrix analysis, we can find the relation between the prism's rotation θ around the z axis and deviation angle ϕ between two gratings (for details see [11]):

$$\delta\phi = 2\theta. \tag{7}$$

Therefore, according to Eq. (6), the roll angle can be obtained using

$$\theta = \arcsin \frac{d}{2w_2} - \arcsin \frac{d}{2w_1}, \tag{8}$$

where w_1 and w_2 are the widths of moiré fringe before and after rotation, respectively.

Figure 4 shows the layout of the optomechanics of the prototype. In the front end, the autocollimation and moiré fringe imaging system share a five-piece achromatic objective lens with minimum distortion, which has a focus length of 400 mm and a diameter of 40 mm. In the center, four BSs, as marked in red, split the optical path into five parts: two emitting subsystems, two imaging subsystems, and a set of eyepieces. The light sources used for grating projection and reticle projection are EVERLIGHT EHP-5393/SUG01 (green) and EHP-5393/SUR01 (red), respectively. The CCD cameras in the imaging subsystems are DALSA Genie HM1400. Gratings and BP filters are customized, and the specific parameters are listed in Table 1.

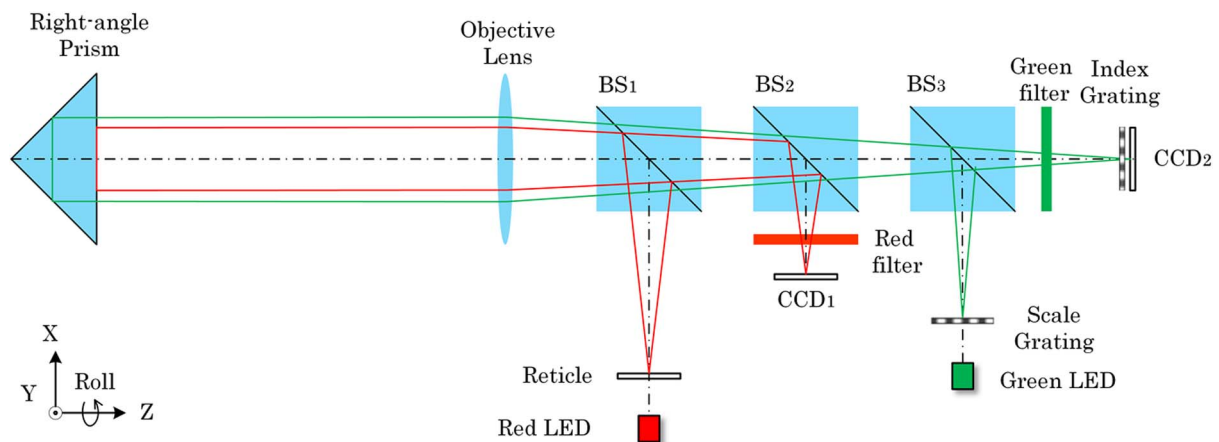


Fig. 3. Simplified optical schematic of the 3D autocollimator.

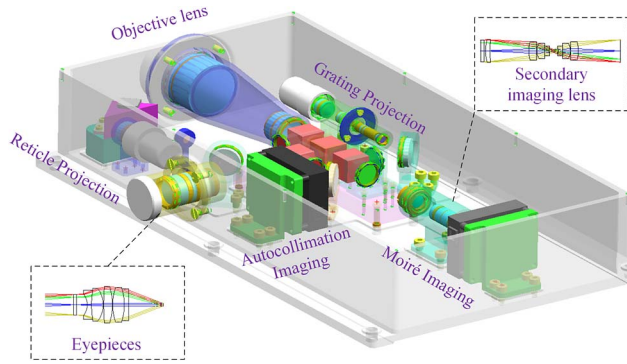


Fig. 4. Layout of the optomechanics of the prototype.

Table 1. Parameters of the Components

Property	Unit	Value
Wavelength of the red LED	nm	620–638
Wavelength of the green LED	nm	520–536
Passband of the red filter	nm	624 ± 4
Passband of the green filter	nm	528 ± 8
Width of the crosshair	µm	100
Size of the crosshair	mm	5 × 5
Grating pitch	µm	50
Grating diameter	mm	9
Pixel size of CCD	µm	7.4 × 7.4
Resolution of CCD	pixel	1400 × 1024

In the moiré imaging subsystem, we originally set the CCD camera (CCD2) right behind the index grating, as shown in Fig. 3, only to find the image to be dim and blurry. Therefore, a secondary imaging lens was designed and mounted between the grating and the camera. Clear images of the moiré fringe were acquired [as shown in Fig. 6(c)].

4. EXPERIMENTS AND RESULTS

To verify the feasibility of the proposed method and evaluate the performance of the prototype, a series of experiments have been performed under the laboratory conditions.

A. Static Calibration for 3D Angle Measurement

Figure 5 is the experimental setup of 3D angle measurement. A right-angle prism along with a cube prism is collinearly

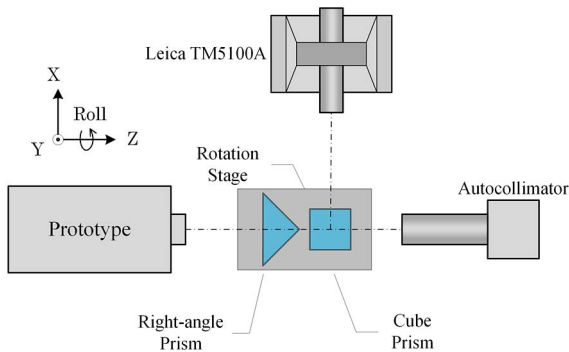


Fig. 5. Experimental setup of the 3D angle measurement.

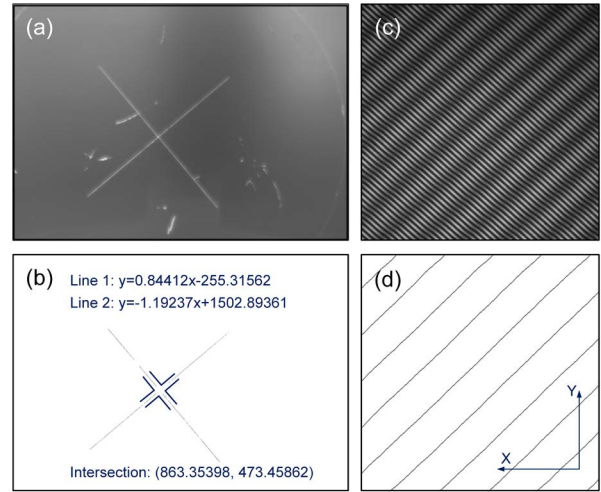


Fig. 6. Image results from the prototype. (a), (b) The crosshair images of autocollimation before and after processing; (c), (d) the images of the moiré fringe before and after processing.

mounted on a high-precision three-axis rotary stage, which provides 3D angular deformation for the test. An industrial theodolite of 0.5 arcsec accuracy (Leica TM5100A) and a standard autocollimator of 0.2 arcsec accuracy (Taylor Hobson DA400) are used in the calibration test. All these instruments and the prototype are set on an optical table to provide a stable environment with minimal deflection.

In the experiment, the 3D angular motion of the stage was indicated by the right-angle prism and measured by the prototype. Simultaneously, on the other end, the pitch and yaw angles were calibrated by the standard autocollimator through one plane of the cube prism. In the vertical direction, the theodolite was facing the other plane and monitoring the roll angle, which to itself is a pitch. Image results from the prototype’s cameras are shown in Fig. 6. The position information of the crosshair image was obtained after a certain image processing series, that is, edge detection, threshold segmentation, line extraction, and calculation of the intersection. Figure 6(b) shows the coordinates of the intersection of crosshair image. Then the values of pitch and yaw can be retrieved using Eq. (3) and (4).

For the moiré fringe image, an image processing series, i.e., low-pass and notch filtering, contrast enhancement, threshold segmentation, and thinning, convert these stripes into single-pixel lines, as shown in Fig. 6(d). If the average lateral spacing between these lines is denoted as x and vertical spacing as y , the width w of the moiré fringe can be obtained using

$$w = \frac{x \cdot y}{\sqrt{x^2 + y^2}} \tag{9}$$

However, as Eq. (8) cannot provide the absolute value of the current roll angle, but rather the rotation relative to its former status, it is important to set a reference (a relative zero) before the roll measurements. So we adjust the stage to ensure the readout of the theodolite is zero and mark the moiré fringe width as w_0 . Then we readjust the stage to produce a roll angle to be measured by the theodolite and the prototype, and the width of the new fringe is recorded as w_1 . Using Eq. (8), the

Table 2. Results of 3D Angle Measurement at 0.3 M

Pitch			Yaw			Roll		
Standard	Prototype		Standard	Prototype		Leica	Prototype	
Autocollimator	Result	Error	Autocollimator	Result	Error	TM5100A	Result	Error
1'48"	1'51"	3	1'35"	1'33"	-2	1'38"	1'42"	4
2'47"	2'45"	-2	2'41"	2'45"	4	2'56"	2'59"	3
4'41"	4'36"	-5	4'15"	4'12"	-3	4'30"	4'22"	-8
6'13"	6'17"	4	6'19"	6'23"	4	5'57"	5'52"	-5
8'28"	8'23"	-3	7'49"	7'52"	3	7'37"	7'43"	6
10'14"	10'18"	4	9'34"	9'31"	-3	9'18"	9'15"	-3
11'39"	11'42"	3	11'11"	11'17"	6	10'51"	10'56"	5
13'13"	13'09"	-4	13'10"	13'08"	-2	12'10"	12'14"	4
14'53"	14'56"	3	14'52"	14'54"	2	13'49"	13'51"	2
16'17"	16'22"	5	16'39"	16'36"	-3	15'09"	15'04"	-5
RMS Error: 3.71"			RMS Error: 3.41"			RMS Error: 4.79"		

current roll angle can be calculated with w_0 and w_1 . In this way, we collect all the measurements of roll one by one.

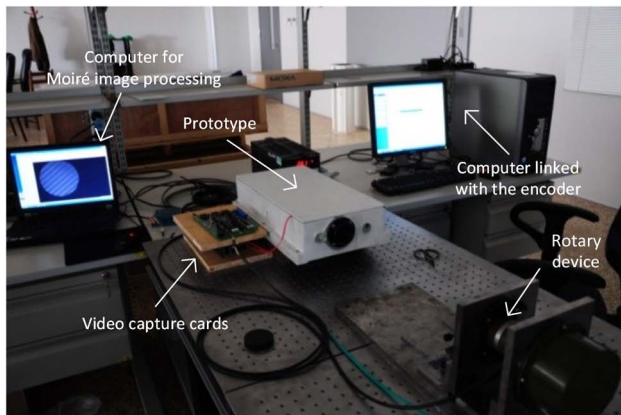
Comparing them to the results from the standard instruments, we have errors as listed in Table 2. When the stage is placed 0.3 m from the prototype, the RMS errors of the measurements are 3.71 arcsec for pitch, 3.41 arcsec for yaw, and 4.79 arcsec for roll. To make the results convincing, we repeat the experiment

at a working distance of 2 m. The results barely change: the RMS errors are 3.83, 3.42, and 4.92 arcsec for pitch, yaw, and roll, respectively. This indicates that the prototype is distance insensitive, which is an appealing advantage in practical applications.

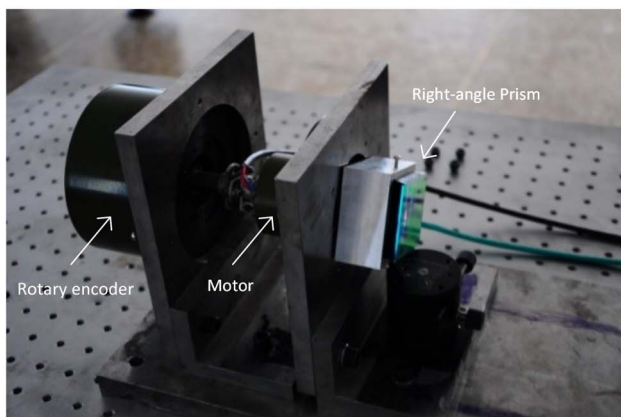
B. Dynamic Roll Angle Measurement

It is conceivable that for some special applications dynamic angle measurements are desirable. Since it is well proved that autocollimators are applicable for dynamic measurements of pitch and yaw angles [5], only the roll measurement is demonstrated here.

As shown in Fig. 7, a self-made rotary device is employed to generate continuous rotation for the test. The device consists of an incremental rotary encoder (21 bit, 0.62 arcsec resolution), a motor, and a right-angle prism attached to it. The motor drives the prism, and the encoder provides a readout of the real-time data of the roll angle at a frequency of 10 Hz. At the same time, the rotation is measured by the prototype interacting with the prism. The images of the moiré fringe are taken by the CCD camera with Sequential Grab Demo (a software tool) at a frequency of 15 frames per second, stored on the computer, and processed afterward. However, as there is no synchronizer for the device and the prototype is not sampling at exactly the



(a)



(b)

Fig. 7. Photograph of the dynamic roll measurement experiment: (a) experimental setup, (b) rotary device.

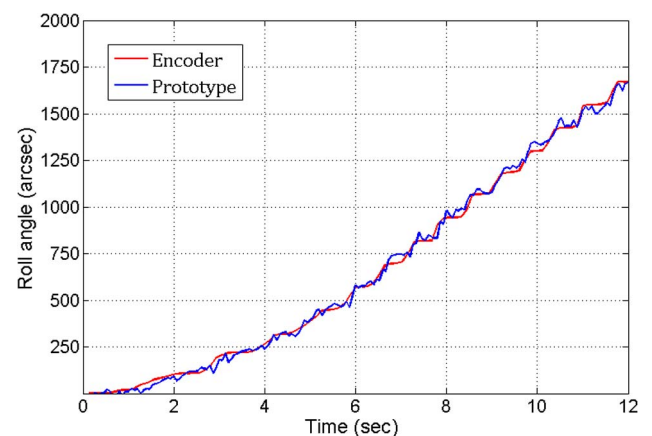


Fig. 8. Results of dynamic roll angle measurement.

same frequency as the encoder, we cannot calculate the errors of the dynamic roll angle measurement, but rather view a general trend of correspondence between the prototype and the encoder. As can be seen in Fig. 8, the continuous rotations are well detected by the prototype.

5. CONCLUSION

In this paper, we have shown that by incorporating moiré technique into a generalized version of an autocollimator, it is possible to perform 3D angle measurement simultaneously. A specially coated right-angle prism is employed as the indicator of angular deformation. The light beam reflected by the hypotenuse of the prism is received by the autocollimation unit for detecting pitch and yaw. Another beam reflected by the two legs of the prism is received by the moiré fringe imaging unit for detecting roll. A 3D autocollimator prototype has been designed, fabricated, and experimentally tested. RMS errors of angle measurements are within 5 arcsec in all 3Ds at a working distance of 2 m. The results are acceptable but not ideal, largely due to manufacturing and assembling errors; thus more work needs to be done to improve the performance. In the future, we will accomplish a high-speed image processing unit and conduct a real-time 3D angle monitoring experiment.

Funding. Jilin Provincial Major Scientific Research Project of China (20150204013GX).

Acknowledgment. The authors acknowledge Dr. Songtao Chang for support in image processing.

REFERENCES

1. F. E. Wright, "A new autocollimator," *J. Opt. Soc. Am.* **9**, 187–188 (1924).
2. R. D. Geckeler, A. Just, M. Krause, and V. V. Yashchuk, "Autocollimators for deflectometry: current status and future progress," *Nucl. Instrum. Methods Phys. Res.* **616**, 140–146 (2010).
3. E. Lubrano and R. Clavel, "Thermal calibration of a 3 DOF ultra high-precision robot operating in industrial environment," in *International Conference on Robotics and Automation* (IEEE, 2010).
4. S. J. Thompson, R. Lang, P. Rees, and G. W. Roberts, "Reconstruction of a conic-section surface from autocollimator-based deflectometric profilometry," *Appl. Opt.* **55**, 2827–2836 (2016).
5. Z. Bian, M. Gao, Z. Dong, Q. Ye, R. Qu, and Z. Fang, "Two-coordinate dynamic photoelectric autocollimator based on single linear CCD," *Proc. SPIE* **7855**, 78550H (2010).
6. J. Yuan and X. Long, "CCD-area-based autocollimator for precision small-angle measurement," *Rev. Sci. Instrum.* **74**, 1362–1365 (2003).
7. V. L. Shur, A. Y. Lukin, Y. N. Shestopalov, and O. I. Popov, "Two-coordinate digital autocollimator," *Meas. Tech.* **48**, 901–906 (2005).
8. I. A. Konyakhin and T. V. Turgalieva, "Three-coordinate digital autocollimator," *J. Opt. Technol.* **80**, 772–777 (2013).
9. Y. Gao, X. Wang, Z. Huang, D. Zhan, and C. Hu, "High-precision rolling angle measurement for a three-dimensional collimator," *Appl. Opt.* **53**, 6629–6634 (2014).
10. W. Gao, Y. Saito, H. Muto, Y. Arai, and Y. Shimizu, "A three-axis autocollimator for detection of angular error motions of a precision stage," *CIRP Ann. Manuf. Tech.* **60**, 515–518 (2011).
11. S. Cai, S. Liang, and Y. Qiao, "Three-dimensional angle measurement based on auto-collimation and Moiré fringe," *Proc. SPIE* **7160**, 716004 (2009).
12. L. Kong, S. Cai, Z. Li, G. Jin, S. Huang, K. Xu, and T. Wang, "Interpretation of Moiré phenomenon in the image domain," *Opt. Express* **19**, 18399–18409 (2011).